Internal Displacement Reactions in Multicomponent Oxides: Part II. Oxide Solid Solutions of Wide Composition Range

S.N.S. REDDY, D.N. LEONARD, L.B. WIGGINS, and K.T. JACOB

As models of internal displacement reactions in oxide solid solutions, the following reactions were studied at 1273 K as a function of time:

$$Fe + (Ni_x Mg_{1-x})O = Ni + (Fe_x Mg_{1-x})O$$
$$Fe + (Co_{0.5} Mg_{0.5})O = Co + (Fe_{0.5} Mg_{0.5})O$$

In both reactions, Ni or Co in the starting oxide is displaced by Fe and the γ-(Ni-Fe) or (Co-Fe) alloy is precipitated. In the reaction zone, composition gradients develop in both product phases, *viz.*, the oxide and the alloy precipitate. The Ni (or Co) concentration of the alloy precipitate increases towards the reaction front. In the product oxide, the "inert" Mg diffuses toward the reaction front along with the Fe, while the Ni (or Co) diffusion is in the opposite direction, towards the Fe/boundary. The shape of the composition profiles for Mg and Fe in the product oxide suggests that cross-coefficient terms in the generalized flux equations contribute significantly to the cation flux. The parabolic rate constants of reactions involving Fe/(Ni_xMg_{1-x})O decrease by nearly four orders of magnitude when x decreases from 1 to 0.1.

I. INTRODUCTION

PREVIOUS studies of solid-state displacement reactions have identified different reaction morphologies and their relationship to the thermodynamic and diffusional transport properties of product phases.[1,2] In the case of simple displacement reactions between a metal and a binary oxide, Rapp *et al.*[1] have predicted the morphologies and reaction rates from a knowledge of the thermodynamic and diffusion data of product phases; the predictions were verified for the following reaction couples: Cu_2O/Ni, Cu_2O/Co, Cu_2O/Fe, and NiO/Fe. Depending on the diffusional rate control in the product phases, the reactive interface is either stable (layered morphology) or unstable (aggregate morphology). The reactive interface is morphologically stable when the rate-controlling diffusion flux is in the same direction as the interface motion (*e.g.*, Cu_2O/Ni and Cu_2O/Co); the interface is unstable when it moves against the rate-determining flux (*e.g.*, Cu_2O/Fe and NiO/Fe). Tangchitvittaya *et al.*[2] have studied the reaction mechanism and the development of an interwoven product morphology for the reaction between Fe and NiO (single-crystal oxide). Internal displacement reactions occur inside a metal or ceramic matrix. The only published internal displacement reaction is between MoO_2 and Cr in a Ni-base alloy matrix by Shook *et al.*[3] As part of a study of internal displacement reactions in multicomponent oxides, a previous study (Part I) considered the reaction between a metal and a ternary oxide compound with a narrow homogeneity range.[4] A study of the internal displacement reaction between a metal and an initially homogeneous single-phase ternary oxide solid solution with a wide composition range, at a constant temperature and pressure, is the subject of this article. In a following article (Part III), oxide solid solutions involving ternary line compounds will be considered.[5]

S.N.S. REDDY, Senior Engineer and L.B. WIGGINS, Senior Technical Staff Member, are with the Systems and Technology Group, IBM Corporation, Hopewell Junction, NY 12533. Contact e-mail: snreddy@us.ibm.com D.N. LEONARD, Graduate Student, is with the Department of Materials Science, North Carolina State University, Raleigh, NC 27695. K.T. JACOB, Professor, is with the Department of Metallurgy, Indian Institute of Science, Bangalore-560012, India.

Manuscript submitted July 13, 2004.

II. AN INTERNAL DISPLACEMENT REACTION IN AN OXIDE SOLID SOLUTION

Consider the oxides **AO**, **BO**, and **CO**, which have the same crystal structure and which form solid solutions in the entire composition range. The thermodynamic stability of the oxides is such that, $\Delta G^{\circ}_{\mathbf{CO}} \ll \Delta G^{\circ}_{\mathbf{AO}} < \Delta G^{\circ}_{\mathbf{BO}}$. The oxide $(\mathbf{B}_x\mathbf{C}_{1-x})\mathbf{O}$ is not stable when in contact with metal **A** at elevated temperatures, and the following internal displacement reaction occurs:

$$x\mathbf{A} + (\mathbf{B}_x\mathbf{C}_{1-x})\mathbf{O} = x\ \text{“}\mathbf{B}\text{”} + \text{“}(\mathbf{A}_x\mathbf{C}_{1-x})\mathbf{O}\text{”};\ \Delta G_1 < 0 \quad [1]$$

The ΔG_1 is the Gibbs energy change for Reaction [1]. During the reaction, cation **B** is displaced by **A** in the oxide without changing the crystal structure of the oxide. The cation **C** does not participate in the chemical exchange reaction. The reaction product phases are typically: "**B**" is an (**A-B**) alloy and "$(\mathbf{A}_x\mathbf{C}_{1-x})\mathbf{O}$" is (**A**,**B**,**C**)**O** solid solution. As the reaction progresses, the reactants are spatially separated from each other by the product phases, as follows:

$$\underset{\text{boundary I}}{\mathbf{A}}\,//\{\underset{\text{reaction zone}}{(\mathbf{A}-\mathbf{B}) + (\mathbf{A},\mathbf{B},\mathbf{C})\mathbf{O}}\}//\underset{\text{boundary II}}{(\mathbf{B}_x\mathbf{C}_{1-x})\mathbf{O}}$$
(**A**/product zone) (reaction front)

Both the product phases exhibit composition gradients in the reaction zone. If the reaction occurs in a single-crystal or polycrystalline oxide with very large grains, the alloy precipitates are isolated when the value of x is small and interconnected for large x values, depending on the morphology.

However, in polycrystalline oxides with small grains, the alloy can be precipitated preferentially along grain boundaries and become interconnected for $x > 0.3$. For very small values of x, the kinetics of Reaction [1] is controlled by cation diffusion in the product oxide. In the following, the diffusion in the alloy phase is neglected from consideration.

The cations **A**,**B** and **C** occupy the same sublattice in the oxide, and their diffusion, involving the same defect mechanism, is correlated. It is assumed that $D_{\mathbf{O}} << D_{\text{cation}}$ and the oxide is electronically conducting with t_e (or t_h) ≈ 1. If the point defects responsible for cation diffusion are vacancies, the flux relationship $\Sigma J_{\text{cation}} = -J_v$ is valid. The displacement Reaction [1] is illustrated schematically in Figure 1.

A. *Chemical Potentials at the Boundaries for Reaction [1]*

In the following discussion, it is assumed that the chemical potentials for **AO**, **BO**, and **CO** in the (**A**,**B**,**C**)**O** solid solution, at a given composition and temperature, are independent of oxygen partial pressure. This is true only when the nonstoichiometry (or defect concentration) in the oxide solid solution is small. Because the oxide (**A**,**B**,**C**)**O** has four components and only two phases (oxide and metal) coexist at any given location, the chemical potentials are not uniquely defined at any location in the reaction zone. However, the relative magnitudes at the boundaries (at boundary I and boundary II) can be specified by assuming chemical equilibrium. The standard states for the chemical potentials of components in the reacting system are assumed to be (at a constant temperature and total pressure) pure **A**, **B**, **C**, **AO**, **BO**, **CO**, and $\mathbf{O}_2$ gas at 1 atmosphere pressure (*e.g.*, $\mu_{\mathbf{A}} = 0$ for pure **A**).

B. *A/Reaction Zone Boundary; Boundary I*

When $\Delta G_1 << 0$, after the start of the initial reaction, the composition of the product oxide at the **A**/boundary is essentially (**A**,**C**)**O** in equilibrium with pure **A** (Figure 1). The oxygen chemical potential at the boundary I is given by ($2\mathbf{A} + \mathbf{O}_2 = 2\mathbf{AO}$) equilibrium as

$$\mu_{\mathbf{A}}^{\mathrm{I}} = 0 \text{ (pure } \mathbf{A} \text{ as the standard state)} \quad [2]$$

$$\mu_{\mathrm{o2}}{}^{\mathrm{I}} = 2\mu_{\mathbf{AO}}{}^{\mathrm{I}} \quad [3]$$

where $\mu_{\mathbf{AO}}$ is the chemical potential of **AO** oxide in (**A**,**C**)**O** solid solution, which is a function of the composition at the boundary. (The superscript I refers to the location as boundary I.) The chemical potentials for **B** and **C** at boundary I are then given by $\mu_{\mathrm{o2}}{}^{\mathrm{I}}$, and the chemical potentials for the oxides are given as

$$2\mu_{\mathbf{B}}{}^{\mathrm{I}} = 2\mu_{\mathbf{BO}}{}^{\mathrm{I}} - \mu_{\mathrm{o2}}{}^{\mathrm{I}} = 2\mu_{\mathbf{BO}}{}^{\mathrm{I}} - 2\mu_{\mathbf{AO}}{}^{\mathrm{I}} \quad [4]$$

$$2\mu_{\mathbf{C}}{}^{\mathrm{I}} = 2\mu_{\mathbf{CO}}{}^{\mathrm{I}} - \mu_{\mathrm{o2}}{}^{\mathrm{I}} = 2\mu_{\mathbf{CO}}{}^{\mathrm{I}} - 2\mu_{\mathbf{AO}}{}^{\mathrm{I}} \quad [5]$$

C. *Reaction Front; Boundary II*

At the reaction front, the metal precipitate is essentially "pure" **B** in contact with the starting oxide, $(\mathbf{B}_x\mathbf{C}_{1-x})\mathbf{O}$, and the oxygen chemical potential is given by (**B** + **BO**) equilibrium:

$$\mu_{\mathbf{B}}{}^{\mathrm{II}} = 0 \quad [6]$$

$$\mu_{\mathrm{o2}}{}^{\mathrm{II}} = 2\mu_{\mathbf{BO}}{}^{\mathrm{II}} \quad [7]$$

where $\mu_{\mathbf{BO}}{}^{\mathrm{II}}$ is the chemical potential of **BO** in $(\mathbf{B}_x\mathbf{C}_{1-x})\mathbf{O}$. Because $\Delta G^{\circ}_{\mathbf{BO}} > \Delta G^{\circ}_{\mathbf{AO}}$, $\mu_{\mathrm{o2}}{}^{\mathrm{II}} > \mu_{\mathrm{o2}}{}^{\mathrm{I}}$. The chemical potentials of **A** and **C** at boundary II are then related to $\mu_{\mathrm{o2}}{}^{\mathrm{II}}$ and the oxide chemical potentials:

$$2\mu_{\mathbf{A}}{}^{\mathrm{II}} = 2\mu_{\mathbf{AO}}{}^{\mathrm{II}} - \mu_{\mathrm{o2}}{}^{\mathrm{II}} = 2\mu_{\mathbf{AO}}{}^{\mathrm{II}} - 2\mu_{\mathbf{BO}}{}^{\mathrm{II}} \quad [8]$$

$$2\mu_{\mathbf{C}}{}^{\mathrm{II}} = 2\mu_{\mathbf{CO}}{}^{\mathrm{II}} - \mu_{\mathrm{o2}}{}^{\mathrm{II}} = 2\mu_{\mathbf{CO}}{}^{\mathrm{II}} - 2\mu_{\mathbf{BO}}{}^{\mathrm{II}} \quad [9]$$

Subtracting the chemical potentials at II from the corresponding values at I gives

$$\mu_{\mathrm{o2}}{}^{\mathrm{I}} - \mu_{\mathrm{o2}}{}^{\mathrm{II}} = 2(\mu_{\mathbf{AO}}{}^{\mathrm{I}} - \mu_{\mathbf{BO}}{}^{\mathrm{II}}) < 0 \quad [10]$$

$$\mu_{\mathbf{A}}{}^{\mathrm{I}} - \mu_{\mathbf{A}}{}^{\mathrm{II}} = \mu_{\mathbf{BO}}{}^{\mathrm{II}} - \mu_{\mathbf{AO}}{}^{\mathrm{II}} > 0 \quad [11]$$

$$\mu_{\mathbf{B}}{}^{\mathrm{I}} - \mu_{\mathbf{B}}{}^{\mathrm{II}} = \mu_{\mathbf{BO}}{}^{\mathrm{I}} - \mu_{\mathbf{AO}}{}^{\mathrm{I}} < 0 \quad [12]$$

$$\mu_{\mathbf{C}}{}^{\mathrm{I}} - \mu_{\mathbf{C}}{}^{\mathrm{II}} = (\mu_{\mathbf{CO}}{}^{\mathrm{I}} - \mu_{\mathbf{CO}}{}^{\mathrm{II}}) + (\mu_{\mathbf{BO}}{}^{\mathrm{II}} - \mu_{\mathbf{AO}}{}^{\mathrm{I}}) = \mathbf{?} \quad [13]$$

In most practical displacement reactions $(\mu_{\mathbf{C}}{}^{\mathrm{I}} - \mu_{\mathbf{C}}{}^{\mathrm{II}}) > 0$, for the reasons discussed in the following.

The second term in Eq. [12], $(\mu_{\mathbf{BO}}{}^{\mathrm{II}} - \mu_{\mathbf{AO}}{}^{\mathrm{I}})$, is always > 0 (positive term), because $\Delta G^{\circ}_{\mathbf{BO}} > \Delta G^{\circ}_{\mathbf{AO}}$. However, the value of the first term, $\{(\mu_{\mathbf{CO}})^{\mathrm{I}} - (\mu_{\mathbf{CO}})^{\mathrm{II}}\}$, can be either 0, >0, or <0, and is related to the thermodynamics of solid solutions, (**A**,**C**)**O** at boundary I and (**B**,**C**)**O** at boundary II. The three distinguishable cases are as follows.

Case (a): $(\mu_{\mathbf{CO}}{}^{\mathrm{I}} - \mu_{\mathbf{CO}}{}^{\mathrm{II}}) = 0$ when $f_{\mathbf{CO}}{}^{\mathrm{I}}$ in $(\mathbf{A}_x\mathbf{C}_{1-x})\mathbf{O}$ = $f_{\mathbf{CO}}{}^{\mathrm{II}}$ in $(\mathbf{B}_x\mathbf{C}_{1-x})\mathbf{O}$, where $f_{\mathbf{CO}}$ is the activity coefficient for **CO** in the solid solutions (standard state is pure **CO**). This means that, for a given concentration, the thermodynamic activities for **CO** are equal in both (**A**,**C**)**O** and (**B**,**C**)**O** solid solutions. Then, $\mu_{\mathbf{C}}{}^{\mathrm{I}} - \mu_{\mathbf{C}}{}^{\mathrm{II}} = (\mu_{\mathbf{BO}}{}^{\mathrm{II}} - \mu_{\mathbf{AO}}{}^{\mathrm{I}}) > 0$.

Case (b): $(\mu_{\mathbf{CO}}{}^{\mathrm{I}} - \mu_{\mathbf{CO}}{}^{\mathrm{II}}) > 0$ when $f_{\mathbf{CO}}{}^{\mathrm{I}}$ in $(\mathbf{A}_x\mathbf{C}_{1-x})\mathbf{O} > f_{\mathbf{CO}}{}^{\mathrm{II}}$ in $(\mathbf{B}_x\mathbf{C}_{1-x})\mathbf{O}$. Then, the thermodynamic activity for **CO** is higher in (**A**,**C**)**O** than in (**B**,**C**)**O** at a fixed **CO** concentration. Both terms in Eq. [12] are positive and

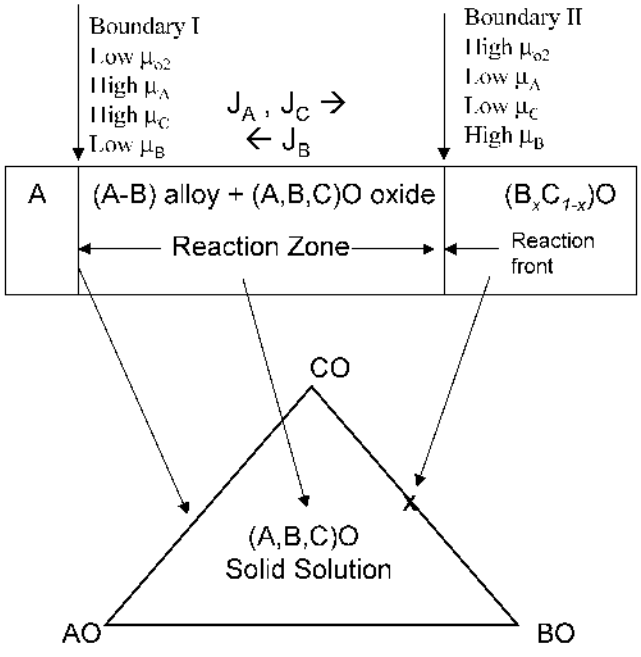

Fig. 1—Internal displacement reaction in an oxide solid solution: x A + $(B_xC_{1-x})O$ = x "B" + "$(A_xC_{1-x})O$".

$(\mu_{\mathbf{C}}^{\mathrm{I}} - \mu_{\mathbf{C}}^{\mathrm{II}}) > 0$; the magnitude of the difference will be larger than in case (a);

Case (c): $(\mu_{\mathbf{CO}}^{\mathrm{I}} - \mu_{\mathbf{CO}}^{\mathrm{II}}) < 0$ when $f_{\mathbf{CO}}^{\mathrm{I}}$ in $(\mathbf{A}_x\mathbf{C}_{1-x})\,\mathbf{O} <$ $f_{\mathbf{CO}}^{\mathrm{II}}$ in $(\mathbf{B}_x\mathbf{C}_{1-x})\mathbf{O}$. Then, Eq.[12] is

$$\mu_{\mathbf{C}}^{\mathrm{I}} - \mu_{\mathbf{C}}^{\mathrm{II}} = (\mu_{\mathbf{CO}}^{\mathrm{I}} - \mu_{\mathbf{CO}}^{\mathrm{II}}) + (\mu_{\mathbf{BO}}^{\mathrm{II}} - \mu_{\mathbf{AO}}^{\mathrm{I}})$$
$$\text{(negative term)} + \text{(positive term)}$$

For most practical internal displacement reactions in oxide solid solutions, $(\mu_{\mathbf{BO}}^{\mathrm{II}} - \mu_{\mathbf{AO}}^{\mathrm{I}}) = (\mu_{o2}^{\mathrm{II}} - \mu_{o2}^{\mathrm{I}}) > |\,(\mu_{\mathbf{CO}}^{\mathrm{I}} - \mu_{\mathbf{CO}}^{\mathrm{II}})\,|$ and, hence, $(\mu_{\mathbf{C}}^{\mathrm{I}} - \mu_{\mathbf{C}}^{\mathrm{II}}) > 0$.

To summarize, for the internal displacement Reaction [1], the chemical potentials at the boundaries are such that $\mu_{\mathbf{A}}^{\mathrm{I}} > \mu_{\mathbf{A}}^{\mathrm{II}}$, $\mu_{\mathbf{B}}^{\mathrm{I}} < \mu_{\mathbf{B}}^{\mathrm{II}}$, and $\mu_{\mathbf{C}}^{\mathrm{I}} > \mu_{\mathbf{C}}^{\mathrm{II}}$. The difference in chemical potentials for **A**, **B**, and **C** at boundaries I and II determines the cation diffusion in the product oxide during the reaction.

The general flux equations for the cation diffusion in the product oxide of Reaction [1], assuming the standard reciprocity condition for transport coefficients, are

$$J_{\mathbf{A}} = -L_{\mathbf{AA}}\nabla\mu_{\mathbf{A}} - L_{\mathbf{AB}}\nabla\mu_{\mathbf{B}} - L_{\mathbf{AC}}\nabla\mu_{\mathbf{C}} \qquad [14a]$$

$$J_{\mathbf{B}} = -L_{\mathbf{AB}}\nabla\mu_{\mathbf{A}} - L_{\mathbf{BB}}\nabla\mu_{\mathbf{B}} - L_{\mathbf{BC}}\nabla\mu_{\mathbf{C}} \qquad [14b]$$

$$J_{\mathbf{C}} = -L_{\mathbf{AC}}\nabla\mu_{\mathbf{A}} - L_{\mathbf{BC}}\nabla\mu_{\mathbf{B}} - L_{\mathbf{CC}}\nabla\mu_{\mathbf{C}} \qquad [14c]$$

In the simplest case, neglecting cross-coefficients, $J_i = -L_{ii}\,\nabla\mu_i$ ($L_{ii} > 0$; i = **A**,**B**,**C**). This gives the flux directions as $J_{\mathbf{A}}$, $J_{\mathbf{C}} \rightarrow$ boundary II, and $J_{\mathbf{B}} \rightarrow$ boundary I (Figure 1). However, because the cations occupy the same sublattice, their diffusion is highly correlated. Hence, the flux terms containing $L_{ij}\nabla\mu_j$ ($i \neq j$) can contribute significantly to J_i, both in magnitude and direction. In general, the cross-coefficients L_{ij} ($i \neq j$), which are functions of oxide composition and oxygen partial pressure, can vary across the reaction zone.*

*For the model displacement reactions considered in this article, *viz.*, Fe/(Ni_xMg_{1-x})O and Fe/(Co_xMg_{1-x})O, it is reasonable to assume that $L_{ij}(i \neq j) > 0$ in the entire reaction zone. However, no experimental information on L_{ij} in (Ni,Fe,Mg)O and (Co,Fe,Mg)O solid solutions is available and the assumption is not proven by empirical data.

When L_{ij} ($i \neq j$) > 0, the following qualitative features of various flux terms in Eq. [14] are noted.

(a) $L_{\mathbf{Ai}}\nabla\mu_{\mathbf{A}}$(i = **A,B,C**) $\rightarrow$ boundary II (reaction front): operative in the entire reaction zone;
(b) $L_{\mathbf{Bi}}\nabla\mu_{\mathbf{B}}$(i = **A,B,C**) $\rightarrow$ boundary I (**A**/boundary): negligible near the **A**/boundary for $\Delta G_1 << 0$; significant near the reaction front; and
(c) $L_{\mathbf{Ci}}\nabla\mu_{\mathbf{C}}$(i = **A,B,C**) $\rightarrow$ boundary II (reaction front): operative in the entire reaction zone.

The composition profile in the product oxide of Reaction [1] should show concentration gradients for all three cations: $N_{\mathbf{A}}$ decreases toward the reaction front, $N_{\mathbf{B}}$ increases toward the reaction front, and the inert cation $N_{\mathbf{C}}$ increases toward the reaction front. In particular, after the start of the Reaction [1], the concentration of the inert cation **C** (which is not participating in the cation exchange reaction) is such that $N_{\mathbf{C}}^{\mathrm{I}} < (1 - x)$ and $N_{\mathbf{C}}^{\mathrm{II}} > (1 - x)$. {The composition of the starting oxide is $N_{\mathbf{C}} = (1 - x)$}. The shape of the concentration profiles inside the reaction zone depends on the relative contribution of various terms in Eq. [14].

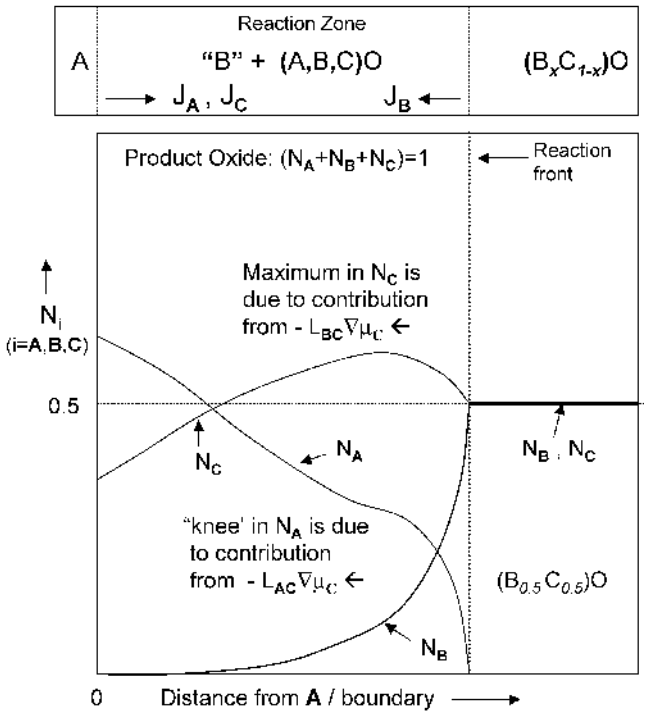

Fig. 2—Schematic composition profile of the product oxide for the reaction: x **A** + $(\mathbf{B}_x\mathbf{C}_{1-x})\mathbf{O} = x$ "**B**" + "$(\mathbf{A}_x\mathbf{C}_{1-x})\mathbf{O}$"; $x = 0.5$ (assumption: $L_{\mathbf{AC}}$, $L_{\mathbf{BC}} > 0$).

One feature of the contribution of cross-coefficient terms may manifest in the concentration profile for inert cation **C** in the reaction zone, when L_{ij} (i = j) > 0. In Eq. [14c], the contribution of $(-L_{\mathbf{AC}}\nabla\mu_{\mathbf{A}} - L_{\mathbf{CC}}\nabla\mu_{\mathbf{C}})$ will result in a monotonic increase of $N_{\mathbf{C}}$ from boundary I to boundary II. However, if the contribution of $-L_{\mathbf{BC}}\nabla\mu_{\mathbf{B}}$ to $J_{\mathbf{C}}$ is significant, $N_{\mathbf{C}}$ will exhibit a maximum inside the reaction zone, probably closer to the reaction front (boundary II). This is related to the direction of the flux term $-L_{\mathbf{BC}}\nabla\mu_{\mathbf{B}}$ (toward boundary I) and is operative near the reaction front, opposing the combined flux from $(-L_{\mathbf{AC}}\,\nabla\mu_{\mathbf{A}} - L_{\mathbf{CC}}\,\nabla\mu_{\mathbf{C}})$. Similarly, in Eq. [14a], the effect of the opposing term—$L_{\mathbf{AC}}\nabla\mu_{\mathbf{C}}$—on $J_{\mathbf{A}}$ should manifest as a "knee" for the concentration profile of **A** inside the reaction zone. A schematic illustration of the composition profile in the product oxide for Reaction [1] is illustrated in Figure 2, under the assumption $L_{ij} > 0$. For illustration purposes, the value of x is chosen as 0.5.

III. REACTION COUPLES Fe/(Ni_xMg_{1-x})O AND Fe/($Co_{0.5}Mg_{0.5}$)O

As models of internal displacement reactions in oxide solid solutions, the following reactions were studied at 1273 K as a function of time:

$$\mathrm{Fe} + (\mathrm{Ni}_x\,\mathrm{Mg}_{1-x})\mathrm{O} = \text{"Ni"} + \text{"}(\mathrm{Fe}_x\,\mathrm{Mg}_{1-x})\mathrm{O}\text{"} \qquad [15]$$

$$(x = 0.7,\ 0.5,\ 0.3,\ 0.2,\ \text{and } 0.1)$$

$$\mathrm{Fe} + (\mathrm{Co}_{0.5}\,\mathrm{Mg}_{0.5})\mathrm{O} = \text{"Co"} + \text{"}(\mathrm{Fe}_{0.5}\,\mathrm{Mg}_{0.5})\mathrm{O}\text{"} \qquad [16]$$

The oxide systems, (Co,Fe,Mg)O and (Ni,Fe,Mg)O, are solid solutions with a rock-salt structure in the entire composition

range. Also, $\Delta G^{o}_{MgO} << \Delta G^{o}_{FeO} < \Delta G^{o}_{CoO} < \Delta G^{o}_{NiO}$. The point defects responsible for cation diffusion are vacancies,[6–9] the concentration of which is a function of composition and oxygen partial pressure at a given temperature. Several studies are available for the thermodynamic activities of MgO in (Ni,Mg)O,[10,11] (Fe,Mg)O,[12–15] and (Co,Mg)O[16–19] solid solutions. The system (Ni,Mg)O is nearly ideal, while (Fe,Mg)O exhibits a positive deviation from ideality in all the studies. The earlier study by Aukrust and Muan[16] of the (Co,Mg)O solid solution indicated near-ideal behavior, and subsequent studies[17,18,19] show a positive deviation from the ideal solution. The deviation from ideality in (Co,Mg)O is less than that for (Fe,Mg)O. As a comparison, from the data for $(Ni_{0.5}Mg_{0.5})O$,[10,11] $(Fe_{0.5}Mg_{0.5})O$,[13,14,15] and $(Co_{0.5}Mg_{0.5})O$,[17,18,19] the following values for μ_{MgO} are estimated (pure MgO as standard state):

For $(Fe_{0.5}Mg_{0.5})O$ in equlibrium with Fe,
$$\mu_{MgO} = -4810 \text{ J/mol};$$

For $(Co_{0.5}Mg_{0.5})O$ in equlibrium with CO,
$$\mu_{MgO} = -6140 \text{ J/mol};$$

For $(Ni_{0.5}Mg_{0.5})O$ in equlibrium with Ni,
$$\mu_{MgO} = -7341 \text{ J/mol};$$

For displacement Reaction [15], between Fe and $(Ni_xMg_{1-x})O$, the chemical potentials at the boundaries (analogous to those in Section II) are as follows.

For the Fe/reaction zone (boundary I),

$$\mu_{Fe}^{I} = 0 \text{ (pure Fe as the standard state)} \quad [14]$$

$$\mu_{o2}^{I} = 2\mu_{FeO}^{I} \quad [15]$$

$$2\mu_{Ni}^{I} = 2\mu_{NiO}^{I} - \mu_{o2}^{I} = 2\mu_{NiO}^{I} - 2\mu_{FeO}^{I} \quad [16]$$

$$2\mu_{Mg}^{I} = 2\mu_{MgO}^{I} - \mu_{o2}^{I} = 2\mu_{MgO}^{I} - 2\mu_{FeO}^{I} \quad [17]$$

where the μ_{oxide} refers to the oxide solid solution at boundary I.

For the reaction front (boundary II),

$$\mu_{Ni}^{II} = 0 \text{ (pure Ni as the standard state)} \quad [18]$$

$$\mu_{o2}^{II} = 2\mu_{NiO}^{II} \quad [19]$$

$$2\mu_{Fe}^{II} = 2\mu_{FeO}^{II} - \mu_{o2}^{II} = 2\mu_{FeO}^{II} - 2\mu_{NiO}^{II} \quad [20]$$

$$2\mu_{Mg}^{II} = 2\mu_{MgO}^{II} - \mu_{o2}^{II} = 2\mu_{MgO}^{II} - 2\mu_{NiO}^{II} \quad [21]$$

Similar relations are valid for Reaction [16] between Fe and $(Co_{0.5}Mg_{0.5})O$, when μ_{Ni} and μ_{NiO} are replaced by μ_{Co} and μ_{CoO}, respectively. Also, based on the available thermodynamic data for solid solutions, for a given value $(1 - x)$ of MgO in the solid solution, μ_{MgO} in (Fe,Mg)O $> \mu_{MgO}$ in (Co,Mg)O $> \mu_{MgO}$ in (Ni,Mg)O. Hence, during Reactions [15] and [16], the directions of cation diffusion are as follows:

$$\mu_{Fe}(\text{Fe/boundary}) > \mu_{Fe}(\text{reaction front}); \; J_{Fe} \rightarrow \text{reaction front}$$

$$\mu_{Mg}(\text{Fe/boundary}) > \mu_{Mg}(\text{reaction front}); \; J_{Mg} \rightarrow \text{reaction front}$$

$$\mu_{Ni}(\text{Fe/boundary}) < \mu_{Ni}(\text{reaction front}); \; J_{Ni} \rightarrow \text{Fe/reaction zone boundary}$$

$$\mu_{Co}(\text{Fe/boundary}) < \mu_{Co}(\text{reaction front}); \; J_{Co} \rightarrow \text{Fe/reaction zone boundary}$$

IV. EXPERIMENTAL PROCEDURE

The starting materials for the preparation of $(Ni_xMg_{1-x})O$ and $(Co_{0.5}Mg_{0.5})O$ solid solutions were powders of NiO (99 pct pure, Cerac, Inc., Milwaukee, WI.), Co_3O_4 (99.7 pct pure, Johnson-Matthey, Ward Hill, MA), and MgO (99.95 pct pure, Johnson-Matthey). The powders, in appropriate ratios, were thoroughly mixed with organics in a three-roll stainless steel mill into paste. The paste was dried in air at 360 K, ground into powder, and pressed as 12-mm discs in a stainless steel die. The discs were slowly heated to 1273 K, to remove all organics and carbon, and were sintered in air at 1873 K, 6 hours for $(Ni_xMg_{1-x})O$, and at 1823 K, 10 hours for $(Co_{0.5}Mg_{0.5})O$. They were then annealed at 1273 K for 240 hours in flowing N_2.

The surfaces of the sintered discs were ground parallel using SiC paper and polished with 3-μm diamond paste. The Fe discs were cut from foil with a purity of 99.995 pct (Puratronic grade, Johnson Matthey); polished with 3-μm diamond paste; and washed ultrasonically in deionized (DI) water just before use.

To start the experiment, Fe/Oxide solid solution discs were sandwiched between two flat alumina plates with a load of 5 kg/cm^2, and placed inside an INCONEL* muffle of the resistance furnace; the reaction couple was surrounded by a "tent" of Cu foil. The atmosphere was flowing high-purity N_2 with less than 1 ppm moisture or O_2. The samples were heated at a rate of 20 K/min to 1273 K, held constant within ± 2 K for a specified time, and cooled to room temperature by turning off the power to the furnace.

The reacted couples were sectioned, mounted, polished, and examined under an optical microscope. Some of the reaction couples were examined in a scanning electron microscope (SEM) and the composition in the reaction zone was analyzed using electron-probe microanalysis (EPMA).

*INCONEL is a trademark of INCO Alloys International, Huntington, WV.

V. RESULTS AND DISCUSSION

A. *Reaction between Fe and $(Ni_xMg_{1-x})O$*

As an example of an internal displacement reaction, Reaction [2] was studied* at 1273 K as a function of ($x = 0.7$, 0.5, 0.3, 0.2, and 0.1) and time; for $x = 0.1$, the reaction was conducted for only one fixed duration of 130 hours. The products of Reaction [15], designated as "Ni" and "$(Fe_xMg_{1-x})O$", are present in solid solutions. The dominating layer is {γNi-Fe) + (Fe,Mg,Ni)O}. For higher values of x, the spinel phase, $(Fe,Mg,Ni)Fe_2O_4$, can form at higher oxygen potentials closer to the reaction front, either as {γ + (Fe,Mg,Ni)O + $(Fe,Mg,Ni)Fe_2O_4$} layer or as {γ + $(Fe,Mg,Ni)Fe_2O_4$} layer. These layers will be referred to as (γ + wustite), (γ + wustite + spinel), and (γ + spinel), respectively, in the discussion that follows. The point defects in (Fe,Mg,Ni)O, responsible for mass transport, are cation vacancies.[6–9] The point defects in the spinel layer, based

*The reaction couple Fe/NiO ($x = 1$) was first studied by Rapp *et al.*,[1] and the mechanism was explored in detail at 1273 K by Tangchitvittaya *et al.*,[2] using single-crystal NiO.

on the data available for Fe_3O_4[20] and Fe-based spinels,[21] are expected to be cation vacancies at high-oxygen activities and cation interstitials at low-oxygen activities. The boundary reactions can be represented as follows.

For the Fe/product zone boundary, the Fe dissolution and cation vacancy annihilation are

$$Fe + V_{cation}(wustite) = Fe^{2+}(wustite) + 2e^{-} \quad [4]$$

For the reaction front, Ni is precipitated along with vacancy generation as

$$Ni^{2+}(wustite) + 2e^{-} = Ni(\gamma) + V_{cation}(wustite) \quad [5]$$

Figures 3 and 4 are cross-sectional views of typical microstructures obtained for the reaction between Fe and $(Ni_xMg_{1-x})O$ at 1273 K. The product zone consists primarily of (γ + wustite for all values of $\tilde{x}$. The γ-alloy phase is continuous and interwoven for $x = 0.7$ and 0.5; the microstructure is similar to that observed for the Fe/NiO reaction.[1,2] For $x = 0.3$, 0.2, and 0.1, the γ phase is larger and elongated along grain boundaries, with smaller discrete particles inside the oxide grains. The importance of grain boundary precipitation is particularly evident for $x \leq 0.3$. The reaction area has substantially less porosity than the starting $(Ni_xMg_{1-x})O$ oxide.

There is no evidence for a distinctly separate (γ + spinel) region formed near the reaction front for $x \leq 0.7$. However, for $x = 0.7$ and 0.5, there is a region containing three phases, (γ + wustite + spinel) near the reaction front, as shown in Figure 5. The spinel phase is probably formed from the oxidation of (Mg,Fe,Ni)O, due to higher oxygen activity closer to the reaction front. The size and amount of the spinel phase, $(Mg,Ni,Fe)Fe_2O_4$, are larger for $x = 0.7$ than for 0.5, and decrease away from the reaction front;

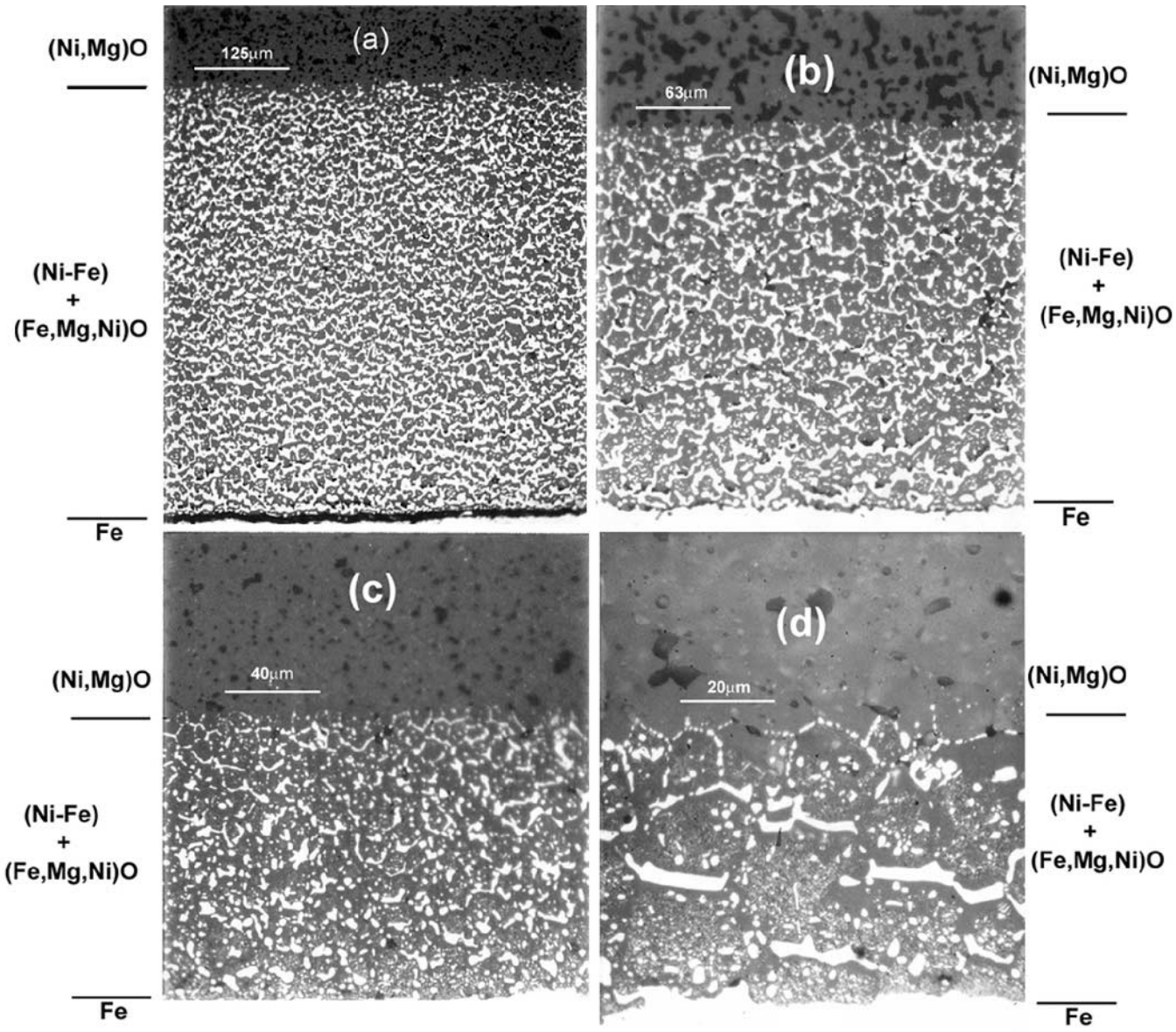

Fig. 3—Cross-sectional view of the reaction zone between Fe and $(Ni_xMg_{1-x})O$ at 1273 K for (*a*) $x = 0.7$, $t = 12$ h; (*b*) $x = 0.5$, $t = 9$ h; (*c*) $x = 0.3$, $t = 25$ h; and (*d*) $x = 0.2$, $t = 49$ h. The bright phase is γ-(Ni,Fe) alloy precipitate.

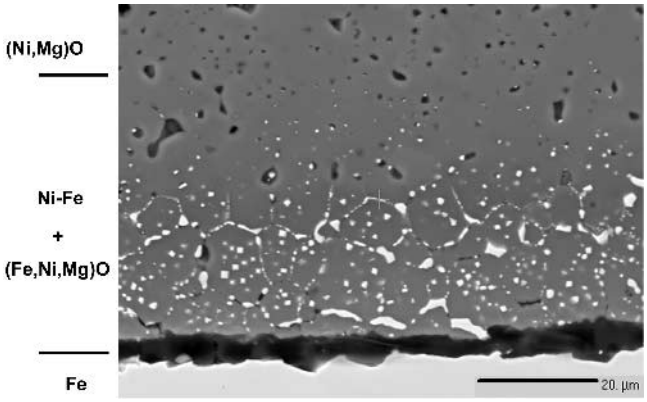

Fig. 4—Reaction between Fe and $(Ni_{0.1}Mg_{0.9})O$ at 1273 K and 130 h, using a cross-sectional SEM image of the reaction zone. The bright phase is γ-(Ni-Fe) alloy precipitate.

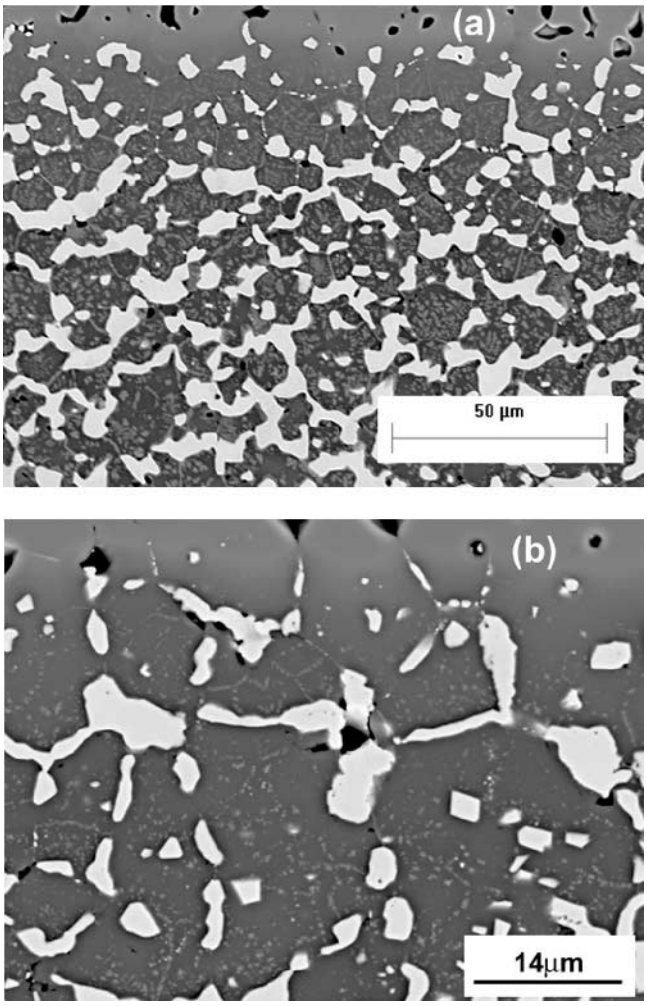

Fig. 5—Fe/$(Ni_xMg_{1-x})O$ reaction at 1273 K and 16 h, using an optical near the reaction front, for (*a*) $x = 0.7$ and (*b*) $x = 0.5$. The bright phase is γ alloy, the dark gray is wustite, and the bright gray is spinel.

none are observed near the Fe/product zone boundary (low μ_{o2} boundary). For $x \leq 0.3$, any presence of spinel near the reaction front was not seen under the optical microscope. Attempts to analyze the composition of the spinel phase,

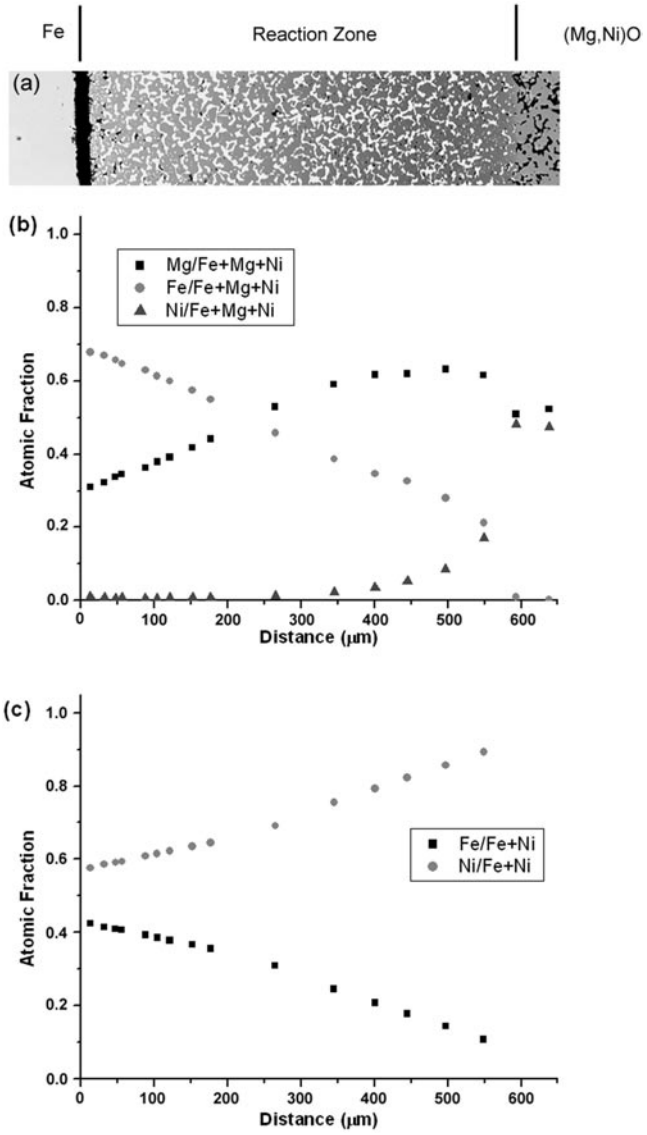

Fig. 6—Reaction between Fe and $(Ni_{0.5}Mg_{0.5})O$ at 1273 K and 81 h, showing (*a*) a cross section of the reaction zone, (*b*) the product oxide (dark phase) composition, and (*c*) the alloy precipitate (bright phase) composition.

for $x = 0.7$ and 0.5, by EPMA without the interference of the neighboring wustite were not successful because of the small size.

The compositions of the product phases, both γ and oxide, across the reaction zone were determined using EPMA and are shown in Figures 6 and 7 for $x = 0.5$ and 0.3. For $x = 0.5$ in Figure 6, the oxide composition near the reaction front is an average of {wustite + spinel (minor amounts)} phases. For convenience, the entire product oxide region in both Figures 6 and 7 will be referred to as a wustite region consisting of (Mg,Fe,Ni)O. Near the Fe/product zone interface, Ni ions are completely displaced by Fe ions in the starting oxide, and the γ precipitate contains about 42 at. pct Fe for $x = 0.5$, and >70 at. pct Fe for $x = 0.3$. Near the reaction front, the γ phase approaches pure Ni in composition.

As expected, the Fe concentration of the product oxide decreases away from the Fe interface; the Ni concentration and its gradient increases as the reaction front is approached.

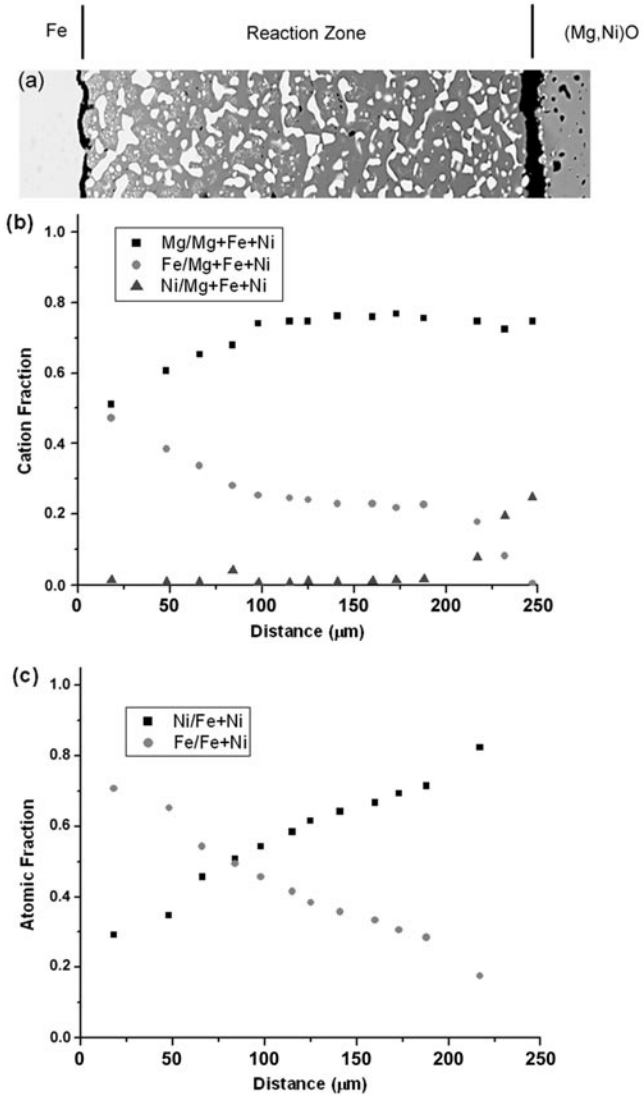

Fig. 7—Reaction between Fe and $(Ni_{0.3}Mg_{0.7})O$ at 1273 K and 110 h, showing (*a*) a cross section of the reaction zone, (*b*) the oxide phase (dark) composition, and (*c*) the alloy phase (bright) composition.

Beyond the reaction front, the composition of the starting $(Ni_xMg_{1-x})O$ is maintained.

The Mg concentration of the product oxide increases away from the Fe interface. In particular, the Mg cation fraction near the Fe/boundary is $<(1-x)$, the value in starting oxide; closer to the reaction front, the value is greater than $(1-x)$. The composition data clearly indicates that, during the internal displacement reaction, there is a flux of Mg cations directed towards the reaction front. As discussed in Section III, this is the result of an increase in μ_{Mg} at the Fe/boundary during the reaction, due to a combination of lower μ_{o2} and higher μ_{MgO} in the (Fe,Mg)O, compared to the corresponding values in (Ni,Mg)O at the reaction front. Based on EPMA results and the thermodynamic activity values in the (Fe,Mg)O and (Ni,Mg)O solid solutions, it is noted that μ_{MgO} (Fe/boundary) $\approx \mu_{MgO}$ (reaction front). However, inside the reaction zone, μ_{MgO} is not constant. In Figures 6 and 7, there is an indication of a maximum in the N_{Mg} inside the reaction zone, ahead

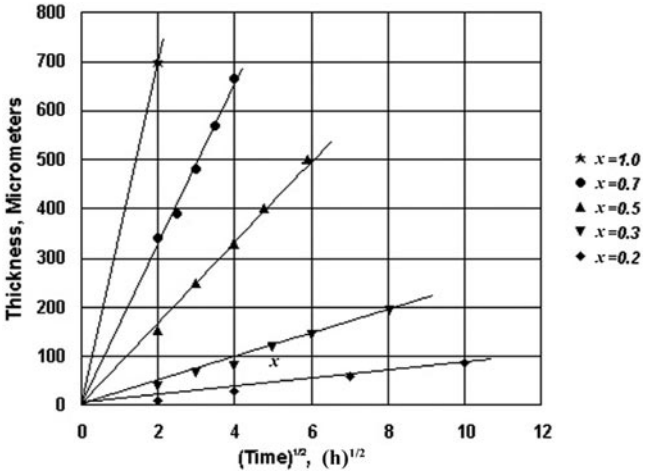

Fig. 8—Kinetics of the displacement reaction between Fe and $(Ni_xMg_{1-x})O$ at 1273 K (data for $x = 1$ from Ref. 2).

Table I. Parabolic Rate Constants for the Reaction x Fe + $(Ni_xMg_{1-x})O$ = x "Ni" + "$(Fe_xMg_{1-x})O$"; T = 1273 K

x	k_p, $m^2\ s^{-1}$
1*	1.7×10^{-11}
0.7	3.8×10^{-12}
0.5	9.6×10^{-13}
0.3	7.7×10^{-14}
0.2	1.0×10^{-14}
0.1	$\sim 2.4 \times 10^{-15}$

*Data for $x = 1$ are from Ref. 2.

of the reaction front, which may be due to the contribution of the cross-coefficient, $L_{NiMg}\ \nabla\mu_{Ni}$, to J_{Mg}, as discussed in Section II.

The presence of a knee in the concentration profile for Fe in the oxide may be an indication of the opposing flux term, $-L_{FeNi}\ \nabla\mu_{Ni}$ to J_{Fe}. However, this observation is not straightforward because of an additional complication due to the presence of both Fe^{2+} and Fe^{3+} in the product oxide. In (Fe,Ni,Mg)O solid solutions of fixed composition, the ratio (Fe^{3+}/Fe^{2+}) increases with increasing oxygen partial pressure (*i.e.*, toward the reaction front) and the coefficients L_{FeFe}, L_{FeNi}, and L_{FeMg} can be different for the two ions. Both the composition (*i.e.*, N_{Fe}) and the oxygen partial pressure are varying across the reaction zone, and the effect of the Fe valence state on the composition profile of the product oxide is not clear.

The kinetics of Reaction [15] at 1273 K, controlled by cation diffusion in the product oxide matrix, follows parabolic behavior and is shown in Figure 8 as the reaction layer thickness *vs* the square root of time. The rate constants, shown in Table I, decrease by about four orders of magnitude when x decreases from 1 to 0.1. The rate constant for $x = 0.1$ is an approximate value, obtained for only one reaction time of 130 hours. Since no data for defects and diffusion in (Mg,Fe,Ni)O are available at 1273 K, it is not possible to relate rate constants and concentration profiles to cation transport in the product oxide. Also, in order to eliminate any grain boundary contribution to kinetics, a study has to be conducted using single-crystal $(Ni_xMg_{1-x})O$.

A. *Reaction between Fe and* $(Co_{0.5}\,Mg_{0.5})O$

Figure 9 represents a cross-sectional view of the reaction between Fe and $(Co_{0.5}Mg_{0.5})O$ at 1273 K. The reaction zone consists of γ-(Co,Fe) alloy and (Fe,Mg,Co)O phases. No other phase was detected, even at high magnification in SEM. The microstructure is similar to that of the Fe/$(Ni_{0.5}\,Mg_{0.5})O$ reaction couple. The composition of the oxide and metal phase in the reaction zone, as determined by EPMA, is shown in Figure 10. Close to the Fe/boundary, the alloy consists of ~45 at. pct Co, and increases to >95 at. pct Co near the

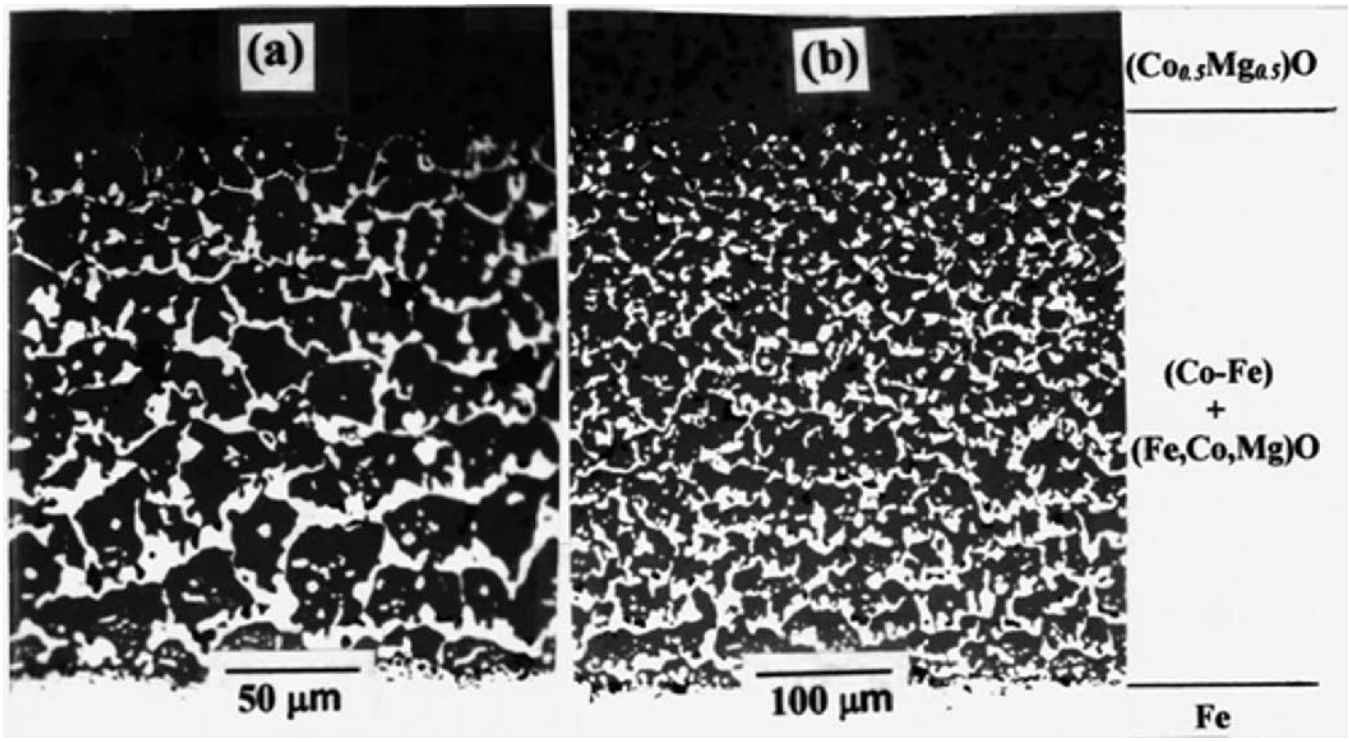

Fig. 9—Displacement reaction between Fe and $(Co_{0.5}Mg_{0.5})O$ at 1273 K for (*a*) 16 h and (*b*) 62 h. The dark phase is (Fe,Co,Mg)O solid solution, and the bright phase is (Co-Fe) alloy precipitate.

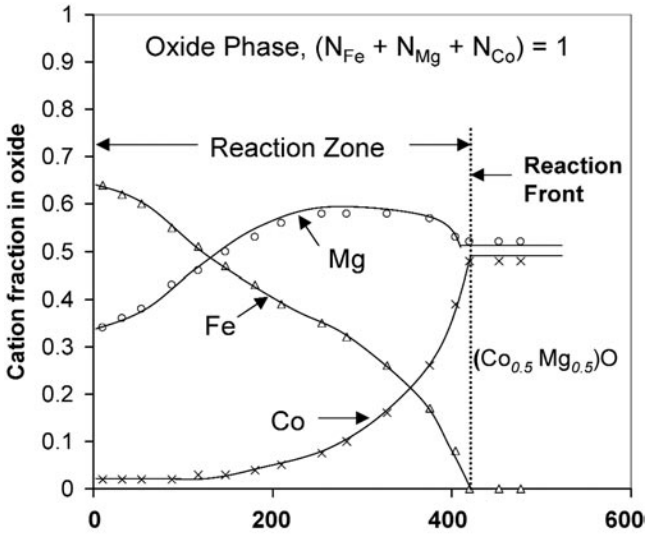

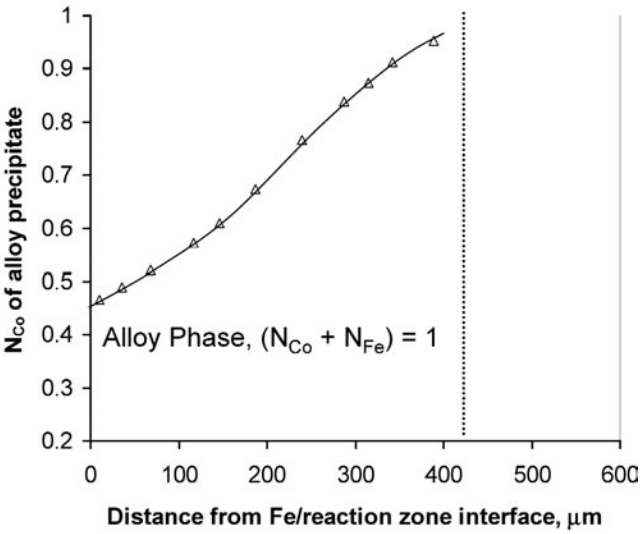

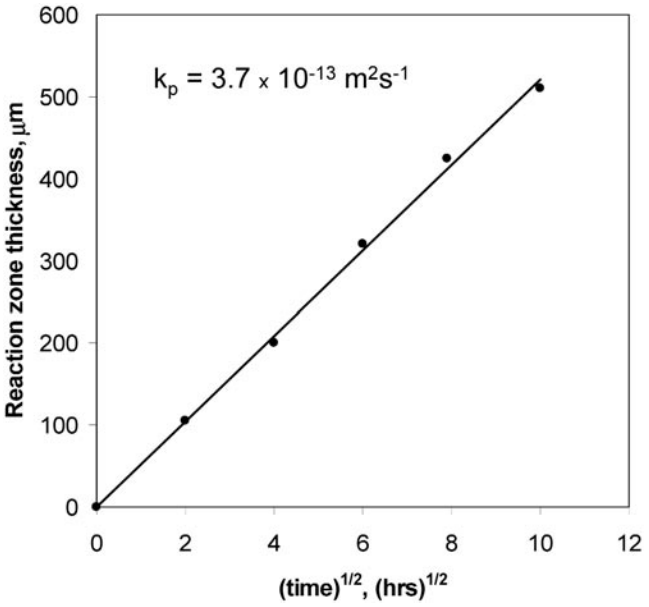

Fig. 11—Kinetics of the displacement reaction between Fe and $(Co_{0.5}Mg_{0.5})O$ at 1273 K.

knee in the Fe concentration profile may be an indication of the $-L_{FeCo}\nabla\mu_{Co}$ contribution to J_{Fe}.

The composition of the oxide beyond the reaction front is constant and is the same as in the starting oxide. The difference in the composition of the starting powder mixture $(Co_{0.5}Mg_{0.5})O$ and the composition given by EPMA $(Co_{0.485}Mg_{0.515})$ is attributed to the measurement errors in EPMA.

The kinetics of the Fe/$(Co_{0.5}Mg_{0.5})O$ reaction at 1273 K is shown in Figure 11 as the reaction layer thickness *vs* $(\text{time})^{1/2}$. The parabolic rate constant is given as $k_p = 3.7 \times 10^{-13}$ m^2 s^{-1}.

VI. SUMMARY

Internal displacement reactions in oxide solid solutions were studied at 1273 K using Fe/$(Ni_xMg_{1-x})O$ and Fe/$(Co_{0.5}Mg_{0.5})O$ reaction couples. During reaction, the Fe displaces Ni (or Co) in the oxide along with the precipitation of the γ alloy. The displacement is nearly complete at the Fe/product zone boundary and decreases towards the reaction front. Concentration gradients develop for both the oxide and the alloy precipitate in the reaction zone.

The γ alloy tends to precipitate along grain boundaries with some small particles inside the grains. The alloy has the highest Fe concentration near the Fe/boundary, and becomes progressively richer in Ni (or Co) toward the reaction front.

During the displacement reaction, as a result of the higher chemical potential for Mg at the Fe/boundary, the inert Mg cation diffuses in the same direction as the Fe, and in a direction opposite to the Ni (or Co). The significance of the contribution by cross-coefficients to the cation flux is qualitatively evident from the concentration profile for the Mg and Fe in the product oxide of the reaction zone.

The reactions follow parabolic kinetics. In the case of the Fe/$(Ni_xMg_{1-x})O$ reaction, the rate constant decreases by about four orders of magnitude when the value of x decreases from 1 to 0.1. Because the transport coefficients in the product oxides are not available, it is not possible to model the concentration profiles and reaction kinetics.

REFERENCES

1. R.A. Rapp, A. Ezis, and G.J. Yurek: *Metall. Trans*., 1973, vol. 4, p. 1283.
2. C. Tangchitvittaya, J.P. Hirth, and R.A. Rapp: *Metall. Trans. A*, 1982, vol. 13A, p. 585.
3. R.L. Shook, R.A. Rapp, and J.P. Hirth: *Metall. Trans. A*, 1985, vol. 16A, p. 1815.
4. S.N.S. Reddy, D.N. Leonard, L.B. Wiggins, and K.T. Jacob: *Metall. Mater. Trans. A*, 2005, vol. 36A, pp. 2685-94.
5. S.N.S. Reddy: *Metall. Mater. Trans. A,* in press.
6. G. Schwier, R. Dieckmann, and H. Schmalzried: *Ber. Bunsenges. Phys. Chem*., 1973, vol. 77, p. 402.
7. R. Dieckmann and H. Schmalzried: *Ber. Bunsenges. Phys. Chem*., 1975, vol. 79, p. 1108.
8. M. Schnehage, R. Dieckmann, and H. Schmalzried: *Ber. Bunsenges. Phys. Chem*., 1982, vol. 86, p. 1061.
9. W.K. Chen and N.L. Peterson: *J. Phys. Chem. Solids*, 1980, vol. 41, p. 335.
10. W.C. Hahn and A. Muan: *J. Phys. Chem. Solids*, 1961, vol. 19, p. 338.
11. S. Mukhopadhayay and K.T. Jacob: *J. Phase Equlibria*, 1995, vol. 16, p. 243.
12. N.G. Schmahl, B. Frisch, and F. Stock: *Arch. Eisenhuttenwes*, 1961, vol. 32, p. 297.
13. W.C. Hahn and A. Muan: *Trans. TMS-AIME*, 1962, vol. 224, p. 416.
14. I. Srecec, A. Ender, E. Woermann, W. Gans, E. Jacobson, G. Eriksson, and E. Rosen: *Phys. Chem. Miner*., 1987, vol. 14, p. 492.
15. P. Wu, G. Eriksson, and A.D. Pelton: *J. Am. Ceram. Soc*., 1993, vol. 76, p. 2065.
16. E. Aukrust and A. Muan: *Trans. TMS-AIME*, 1963, vol. 227, p. 1378.
17. S. Seetharaman and K.P. Abraham: *J. Electrochem. Soc. India*, 1971, vol. 20, p. 54.
18. M. Rigaud, G. Giovannetti, and M. Hone: *J. Chem. Thermodyn*., 1974, vol. 6, p. 993.
19. K.T. Jacob, S. Mukhopadhayay, and A.K. Shukla: *J. Am. Ceram. Soc*., 1992, vol. 75, p. 3081.
20. R. Dieckmann and H. Schmalzried: *Ber. Bunsenges. Phys. Chem*., 1977, vol. 81, p. 344.
21. Sun-Ho Kang and Han-Ill Yoo: *J. Solid State Chem*., 1998, vol. 139, p. 128.